Intravenous administration of scAAV9-Hexb normalizes lifespan and prevents pathology in Sandhoff disease mice

Natalia Niemir[1,2,*], Laura Rouvière[1,2,*], Aurore Besse[3], Marie T. Vanier[4], Jasmin Dmytrus[5], Thibaut Marais[3], Stéphanie Astord[3], Jean-Philippe Puech[6], Ganna Panasyuk[1,2], Jonathan D. Cooper[5,7], Martine Barkats[3,#] and Catherine Caillaud[1,2,6,#]

[1] INSERM U1151, Institut Necker Enfants Malades, Paris 75014, France

[2] Université Paris Descartes, Sorbonne Paris Cité, Paris, France

[3] Centre of Research in Myology, Institut de Myologie, Sorbonne Universités, UPMC University Paris 06, Inserm UMRS974, GH Pitié Salpêtrière, Paris 75013, France

[4] INSERM U820, Lyon 69372, France

[5] Department of Basic and Clinical Neuroscience, King's College London, Institute of Psychiatry, Psychology & Neuroscience, Maurice Wohl Clinical Neuroscience Institute, London SE5 9RX, UK

[6] Service de Biochimie, Métabolomique et Protéomique, Hôpital Universitaire Necker-Enfants Malades, Assistance Publique-Hôpitaux de Paris, Paris 75015, France

[7] Department of Pediatrics, Los Angeles Biomedical Research Institute, David Geffen School of Medicine, UCLA, Torrance, CA 90502, USA

[*] These authors contributed equally to this work

[#] Co-senior authors

Correspondence should be addressed to:

Dr Catherine CAILLAUD, INSERM U1151, Institut Necker-Enfants Malades, 14 rue Maria Helena Vieira da Silva, 75993 PARIS Cedex 14, France. Phone : +33 1 71 39 69 74, Fax : +33 1 44 49 51 30, E-mail: catherine.caillaud@inserm.fr

ABSTRACT

Sandhoff disease (SD) is a rare inherited disorder caused by a deficiency of β-hexosaminidase activity which is fatal because no effective treatment is available. A mouse model of *Hexb* deficiency reproduces the key pathognomonic features of SD patients with severe ubiquitous lysosomal dysfunction, GM2 accumulation, neuroinflammation and neurodegeneration, culminating in death at 4 months. Here, we show that a single intravenous neonatal administration of a self-complementary adeno-associated virus 9 vector (scAAV9) expressing the *Hexb* cDNA in SD mice is safe and sufficient to prevent disease development. Importantly, we demonstrate for the first time that this treatment results in a normal lifespan (over 700 days) and normalizes motor function assessed by a battery of behavioral tests, with scAAV9-treated SD mice being indistinguishable from wild-type littermates. Biochemical analyses in multiple tissues showed a significant increase in hexosaminidase A activity, which reached 10-15% of normal levels. AAV9 treatment was sufficient to prevent GM2 and GA2 storage almost completely in cerebrum (less so in cerebellum), as well as thalamic reactive gliosis and thalamocortical neuron loss in treated *Hexb*-/- mice. In summary, this study demonstrated a widespread protective effect throughout the entire CNS after a single intravenous administration of scAAV9-Hexb vector to neonatal SD mice.

INTRODUCTION

Sandhoff disease (SD) is one of sixty lysosomal storage disorders (LSDs) that, collectively, are common inborn errors of metabolism. This disorder is caused by mutations in the *HEXB* gene encoding the hexosaminidases β-chain and results in deficiency of β-hexosaminidases A and B activity and abnormal catabolism of GM2 ganglioside leading to storage of GM2 and other glycosphingolipids in brain and other organs (1). Clinically, patients affected by SD present with developmental regression, neurological and motor deterioration, blindness, seizures and a cherry-red spot in the retina (2, 3). SD is a severe disease culminating in death before the age of 2 years, and there is a pressing need to develop effective and long-lasting therapies. The *Hexb-/-* mouse model mimicks the biochemical defect of SD with a widespread accumulation of GM2 ganglioside and GA2 glycolipid in the central nervous system (CNS) (4, 5). Symptomatically, mice develop a severe neurological phenotype including motor abnormalities and seizures, and a peripheral storage with marked liver hypertrophy resulting in death around 4 months. The neurodegenerative phenotype of *Hexb-/-* mice is pronounced and includes profound neuroinflammation and neuronal apoptosis (6–8).

Different therapeutic approaches including bone marrow transplantation, enzyme replacement, substrate reduction and chaperone-mediated stabilization of the mutant enzyme have been tested in SD mice, but have shown limited efficacy (7, 9–11). Gene therapy is an attractive therapeutic option for this monogenic genetic disease and direct brain delivery of recombinant adeno-associated virus (AAV) reduced CNS levels of GM2 storage and prolonged survival in SD mice, but its overall efficacy was limited by the persistence of disease in peripheral organs (12, 13). As such, the development of vectors efficient for combined CNS and systemic targeting has proved a challenge for SD. Recombinant AAV9 vectors are promising tools due to their capacity to deliver a transgene to brain after neonatal intravenous administration (14, 15). Moreover, their high neuronal tropism and long-lasting

gene expression are particularly attractive. Indeed, their efficacy in reverting neurological phenotypes has already been demonstrated in mouse model of spinal muscular atrophy (16–18), as well as in different LSDs (19–22). Additionally, AAV9 vectors delivered into the bloodstream efficiently transduce several peripheral tissues, including liver and heart, demonstrating the ability to target pathology in somatic tissues (14, 23). Recent reports using AAV9-based gene therapy in SD mice have provided proof of principle that intravenous administration could be an option in this disorder, but they led to only partial restoration of storage burden and resulted in a moderate impact upon lifespan (24, 25).

Here, we demonstrate the long-term therapeutic efficacy of a specific self-complementary AAV9 (scAAV9-Hexb) vector via single intravenous injection in the SD murine model. We conducted a thorough pathophysiological assessment including multiple behavioral tests performed weekly over a 2 year period, biochemical analyses of lysosomal function and GM2 storage, histological analyses of brain pathology, all showing a remarkable therapeutic efficiency of scAAV9-Hexb. In conclusion, our work provides a strong rationale for single intravenous administration of scAAV9 being an efficient, safe and relatively non-invasive approach for treatment of GM2 gangliosidoses and potentially other neurodegenerative diseases.

RESULTS

scAAV9-Hexb treatment partially restores β-hexosaminidase activity in SD mice

First, a recombinant scAAV9 vector expressing a cDNA of mouse β-hexosaminidase β-subunit under the control of the constitutive phosphoglycerate kinase (PGK) promoter (scAAV9-Hexb) was generated. Purified scAAV9-Hexb viral vectors were injected intravenously in *Hexb-/-* mice at neonatal period (D1-D2) at the dose of 3.5 x 10^{13} vector genomes (vg)/kg. The level of total Hex A+B and specific Hex A enzyme activities were analysed in brain, brainstem and liver of treated mice by comparison with naive SD mice and

wild-type (WT) mice at two months (early symptomatic stage) and four months (terminal stage) of age using MUG and MUGS artificial substrates, respectively. A single intravenous administration of scAAV9-Hexb vector led to a significant increase in both Hex A+B and specific Hex A activities by comparison with naive SD mice (Figure 1A-F). In the forebrain, the activity of hexosaminidase A reached a level around 15% of normal (Figure 1B). The results in brainstem (showing high residual activity of the deficient enzyme in untreated mice) need to be interpreted with caution due to the low quantity of tissue available for the assay (Figure 1D). In the liver, Hex A was around 10% of normal (Figure 1F). It is important to note that vg (vector genome) copy number was evaluated by qPCR using primers specific for *Hexb* cDNA and beta-globin as control gene. It was around 1 in cerebrum and 10 in liver (data not shown).

Normalization of lysosomal function in SD mice by scAAV9-Hexb treatment

In addition to the primary enzyme deficiency, secondary increases in the activity of other lysosomal enzymes is commonly observed in LSDs and can be used as a surrogate marker of lysosomal function (26, 27). To determine if administration of scAAV9-Hexb vector normalises lysosomal function, activities of lysosomal enzymes β-glucuronidase, α-fucosidase and β-galactosidase were tested using specific fluorogenic substrates in brain and brainstem tissues collected at the same ages (Figure 2A,B). In untreated SD mice, these enzymatic activities (expressed as % of WT) were highly elevated, with each reaching up to ten times the normal level. Importantly, treatment with scAAV9-Hexb led to a significant decrease in activities of these enzymes in brain and brainstem.

Neuron morphology and lysosomal mass are normal in treated SD mutants

As lipid storage is a major hallmark of SD, we next investigated the effect of scAAV9-Hexb treatment on this aspect of the disease pathophysiology. First, Nissl staining revealed that in 4-month old *Hexb-/-* mice neuron morphology was abnormal with their cell soma enlarged and filled with pale storage material that displaced the Nissl staining of the cytoplasm within cells in all areas of the brain analyzed (Figure 2C). Conversely, scAAV9-Hexb-treated animals showed complete correction of this pathological accumulation within cells throughout the brain. In addition, immunostaining for lysosomal-associated membrane protein 1 (LAMP-1) was used to indirectly evaluate the storage burden and as a general marker of lysosomal dysfunction in SD mutants, as it has previously been used in other LSD models (21, 28, 29). Pronounced intracellular accumulation of LAMP-1 within numerous regions such as hypothalamus, cortex and hippocampus was observed in brain of 4-month old *Hexb-/-* animals (Figure S1). Furthermore, higher magnification revealed cell bodies with intense LAMP-1 immunostaining throughout the entire section (Figure 2D). Importantly, this pathologic upregulation of LAMP-1 was completely normalized with scAAV9-Hexb treatment to a level comparable to that observed in control littermates.

GM2/GA2 storage in SD mutants is prevented by β-hexosaminidase expression

To further evaluate the effect of therapy on the primary lipid storage in brain, biochemical analysis of GM2 ganglioside and its asialo counterpart gangliotriaosylceramide (GA2) was performed on cerebral and cerebellar tissues of WT, untreated and scAAV9-treated Sandhoff mice at 2- and 4-months of age (Figure 3A-C). The developmental pattern of GM2 (expressed as % of total gangliosides) between 7 and 120 days was further studied in cerebrum of Sandhoff and WT mice (Figure 3B). In WT mouse brain, GM2 is a very minor compound (less than 2.3% of total gangliosides at all ages). Conversely, as can be seen from thin-layer chromatographic profiles of total gangliosides (Figure 3A) and their quantitative evaluation

(Figure 3B), in cerebrum of Sandhoff mice, GM2 is already greatly abnormal at 7 postnatal days (~12% of total gangliosides) and its proportion raises very rapidly, to reach 17, 35 and 40% at 2 weeks, 2- and 4 months of age, respectively. Although the distribution of major ganglioside species is different in cerebellum from that in forebrain, a massive GM2 storage (40 and 48% at 2 and 4 months) also occurs in Sandhoff mice. By contrast, scAAV9-driven expression of Hex B was sufficient to almost completely prevent this pathological accumulation of GM2 in forebrain of age-matched treated Sandhoff mice (4.3±0.3% at 4 months of age), with similar although less pronounced reduction in their cerebellum (global mean/SD 14.4±2.6%) (Figure 3A,B). Further, GA2 - a glycolipid virtually absent in brain of WT mice but showing a many-fold increase in Sandhoff disease - was also undetectable in the cerebrum of scAAV9-treated Sandhoff mice at 2- and 4-months post-injection, and vastly reduced in cerebellum (Figure 3C).

scAAV9-Hexb prevents thalamocortical neuropathology in SD mice

As in many other LSDs, a key neuropathological landmark of SD is profound glial activation and neuron loss within the somatosensory thalamocortical system of *Hexb-/-* mice (Pressey S, *unpublished data*). In order to evaluate the impact of scAAV9-Hexb treatment on the onset and progression of this pathology, neuropathological analyses were conducted on the somatosensory barrelfield cortex (S1BF) and the ventral posterior thalamic nuclei (VPM/VPL) that project to this region of cortex (Figure 4A). Immunostaining for the astrocyte marker GFAP (glial fibrillary acidic protein) revealed pronounced astrocytosis in both VPM/VPL and S1BF of untreated *Hexb-/-* mice, that was already present at 2 months of age and worsened with increased age (Figure 4B). Remarkably, the distribution of GFAP immunoreactivity within the thalamus of scAAV9-treated mice was comparable to age-matched WT animals, including not only the most severely affected VPM/VPL, but also the

adjacent visual relay nucleus LGNd that typically displays a later onset of astrocytosis (Figure S2A). Similar effects of scAAV9-Hexb were evident in the cortex of treated mutant mice with astrocytosis virtually abolished (Figure 4D). All these results were confirmed by quantitative threshold image analysis (Figure 4C,E).

Next, microglial activation was quantified by CD68 immunostaining in the thalamus and cortex of control and scAAV9-treated SD mice, which revealed progressive microglial activation in the thalamocortical system that was more localized compared to astrocytosis (Figure 5A and 4B). In marked contrast, the intensity and distribution of CD68 immunostaining in both the thalamus (Figures 5A,B and S2B) and cortex (Figure 5C,D) of scAAV9-treated *Hexb-/-* mice were indistinguishable from that seen in WT animals at both ages analyzed. Finally, in order to assess if this scAAV9-Hexb treatment also protect neurons from dying, unbiased optical fractionator counts of Nissl stained neurons were made in thalamic VPM/VPL across all treatment groups. There was a profound and significant loss of VPM/VPL neurons in untreated SD animals compared to WT mice (Figure 5E), but this was almost completely prevented in scAAV9-treated mice, suggesting a pronounced therapeutic effect of this vector upon vulnerable neuronal populations within the thalamocortical system of SD mice.

Absence of neuroinflammation in other CNS regions in scAAV9-treated SD mice

In order to determine how widespread the impact of scAAV9-Hexb treatment upon neuropathology is, we performed similar analyses of glial activation and neuron loss in brainstem and cerebellum, two other brain regions also profoundly affected by SD. Within the brainstem, this analysis focussed upon the reticular formation (RF) and spinal trigeminal nucleus V (SPV) (Figure 6A; dotted area 2 and 3), and within the cerebellum upon the deep cerebral nuclei (DCN), and the molecular and granular layers of the cerebellar cortex and

white matter (Figure 6A; dotted area 1 and inset 4). GFAP-immunostaining in untreated *Hexb-/-* mice revealed that, as disease progressed, astrocytosis became more pronounced in all the brainstem and cerebellar regions analysed (Figures 6 and S3), with astrocytes becoming more intensely stained and hypertrophied with increased age. Remarkably, this astrocytosis was completely prevented in both the brainstem (SPV and RF) (Figure 6B,D) and cerebellum (Figure S3A,B,E,F) of AAV9-treated SD mice at 2- and 4-months. This was also confirmed by quantitative threshold image analysis (Figures 6C,E and S3C,D,G,H).

Pronounced CD68 immunoreactivity was also found in the same brainstem and cerebellar regions of 2- and 4-month old *Hexb-/-* mice (Figures 7A,B and S4A,B,E,F), with changes in staining intensity and cellular morphology suggesting progressive microglial activation in these brain regions. In marked contrast, CD68 stained sections from scAAV9-treated *Hexb-/-* mice appeared comparable to age-matched WT mice, with a near complete prevention of microglial activation in these treated mutant mice as confirmed quantitatively (Figures 7C,D and S4C,D,G,H). Finally, to measure the impact of treatment on neuron survival, neuron counts were performed at 4 months of age in one brainstem (SPV) and one cerebellar region (DCN). Neuron counts in both regions showed that the significant loss of Nissl-stained neurons usually seen in the brainstem and cerebellum in untreated *Hexb-/-* mice was prevented by scAAV9-treatment (Figure 7E,F).

scAAV9-Hexb treated SD mice have normal lifespan and locomotor function

Given the positive effect of scAAV9-Hexb treatment on biochemical and pathological measures of disease, long-term life expectancy was evaluated in AAV9-treated SD mice by comparison with untreated SD and WT mice. Compared to the average 750 day lifespan of WT mice, untreated *Hexb-/-* mice displayed a significantly shorter average lifespan of 117 days (Figure 8A). Notably, the survival of SD mutants treated with scAAV9-Hexb was

significantly extended and was completely comparable to that of WT mice (mean >750 days). Furthermore, these scAAV9-injected SD mice were also phenotypically undistinguishable from control WT mice and did not display the characteristic tremor evident in murine SD (Video S1). In addition, while the weight of untreated SD mutants rapidly decreased by about 40% between 14-16 weeks coinciding with aggravation of their pathological phenotype, the weight of AAV9-treated SD mice did not decrease over time, but remained stable reflecting a maintenance of feeding ability comparable to WT mice (Figure 8B).

To evaluate locomotor skills in scAAV9-treated SD mice, a range of behavioral tests were performed on each animal on a weekly basis. Mice were first submitted to the inverted screen test and the latency to fall from the returned metal grid was recorded. At the beginning of the testing period (from 8 to 12 weeks), mice from all three groups were undistinguishable in their ability to stay on the grid (Figure 8C). However, starting from 12 weeks of age *Hexb-/-* mice developed a progressive loss of muscular strength, and the time they could remain on the grid progressively decreased, finally reaching zero due to complete paralysis at 16 weeks (Figure 8C). In contrast, the performance of scAAV9-treated SD mice in this test was identical to WT mice throughout the entire duration of the experiment (>750 days). As a further measure of their physical performance and motor coordination, mice were also assessed using an accelerating rotarod. The latency of untreated Sandhoff mice to fall was dramatically and significantly reduced with disease progression, whereas scAAV9-treated SD mice were completely comparable to normal at all timepoints tested (Figure 8D). The gait of mice from all treatment groups was also evaluated using a painted footprint test (Figure S5). *Hexb-/-* mice showed significant paralysis and characteristic dragged pattern of their footprints due to reduced muscular strength and impaired neurological function at 4 months (Figure S5). However, scAAV9-treated SD animals behaved similarly to WT at 4, 12, 16 and 20 months with no overt gait aberrations. Finally, mice locomotion was evaluated in the

home-cage environment using an activmeter. The test was conducted at 2, 4, 8, 12, 16 and 20 months in treated SD and WT mice, and at 2 and 4 months in naive Sandhoff mice which showed a dramatic and significant decline in all parameters. By contrast, global movement (time in movement and distance covered) was not significantly different between WT mice and scAAV9-treated *Hexb-/-* mice (Figure S6A,B).

DISCUSSION

Here we report for the first time a systemic gene therapy approach that results in normal lifespan and quality of life in a murine model of Sandhoff disease, in addition to almost completely preventing a series of disease-associated biochemical and neuropathological changes. A single intravenous administration of scAAV9-Hexb vector in neonatal mice was sufficient to provide global transduction and widespread therapeutic effect throughout the entire CNS. Targeting this organ enabled therapeutic correction of key features of SD including Hexb enzymatic deficiency itself, lysosomal dysfunction, GM2 and GA2 storage, neuroinflammation and neuronal loss that is seen in patients and reproduced in SD mice.

Our protocol of administering a scAAV9-based vector to neonates is based on several considerations. *Hexb-/-* mice after a latent phase of their disease undergo a rapid decline culminating in death around 16 weeks of age (5). However, GM2 storage is already present in the brain of 7-day old *Hexb* mutants (Figure 3B). A low level of astrocytosis and microglial activation is also evident in 1-month old SD mice (unpublished data). As behavioural symptoms of the disease, like head tremor, are visible around 10 weeks, the development of an early intervention is crucial. For this reason, the scAAV9 therapeutic vector was administered 1-2 days after birth and this vector was specifically used, as this serotype is able to cross the blood-brain barrier (BBB) and self-complementary vector allows rapid maximal transgene expression. Interestingly, a differential targeting of cell types has been observed in

the CNS after intravenous delivery of scAAV9 vectors depending on the age of administration. In neonates, systemic injection resulted in widespread transduction with an apparent tropism toward neurons while transduction of predominantly astrocytes was seen in adult animals (15). Importantly, correction of SD symptoms in multiple brain regions that we report here, strongly suggest that scAAV9-Hexb vector efficiently transduced neurons that are mainly involved in Sandhoff disease effectively preventing their degeneration. In addition, secretion of active β-hexosaminidase by transduced neurons with subsequent recapture by distant cells likely contributes to the widespread correction observed in SD mice (30). It is important to note that treatment in mice at postnatal day 1-2 corresponds to a second trimester of human embryonic growth (31, 32). As such, in order to translate these encouraging results to clinic, a feasibility and tolerability of our approach is now being tested in symptomatic SD mice to provide a more realistic approximation of treating children diagnosed with SD.

We show here for the first time a long-term rescue of GM2 gangliosidosis, not only in the forebrain, but also in more caudal parts of the brain (cerebellum and brainstem) after scAAV9-mediated gene transfer in the acute Sandhoff mouse model. Of note, residual accumulation of GA2 and GM2 lipids was still observed in cerebellum of scAAV9-Hexb treated mice suggesting that this region is possibly less well targeted by AAV9, as recently shown by comparison with AAV10 (33). Future studies will need to address this apparently unequal transduction efficiency in different brain regions in order to optimise this therapeutic strategy. It was stated that the dose of scAAV9 required to achieve effective transduction via systemic vascular delivery in adult mice was approximately 1.0×10^{13} vg/kg (34, 35). In our study, the dose of scAAV9-Hexb vector (3.5×10^{13} vg/kg) induced prolonged expression of β-hexosaminidase transgene without cytotoxicity and therapeutic vector expression was stable in the long-term. Extraordinarily, scAAV9-Hexb treated SD mice survived beyond 2 years of age (mean survival >700 days) without manifesting any signs of disease. Although long-term

survival of SD mice following intravenous delivery of AAV9-Hexb in neonates has been reported (24), at the age of 43 weeks 80% treated SD mutants had developed liver and lung tumors, most likely due to the comparatively high dose of AAV used (2.5 x 10^{14} vg/kg). In contrast, in our study using a lower dose, with its dramatically better treatment outcomes, there was no evidence of malignancies neither in WT nor in injected SD mice via macroscopic examination performed at the experimental end-point in 2-year old animals (data not shown). These data suggest that the choice of the vector (scAAV9 versus rAAV9) and the lower dose used in our study contribute to the long-term outcomes of treatment in murine SD and to the absence of deleterious effects previously reported (24) and recently discussed by Chandler *et al* (36).

It has previously been shown in adult SD mice that intrastratial delivery of recombinant adeno-associated viral vectors (rAAV2/1) expressing either the human β-subunit alone or both α and β subunits delayed their disease (12). However, administration to 1-month-old *Hexb-/-* mice of both rAAVα + rAAVβ enabled an abundant expression of Hex A and Hex B, but a single rAAVβ infusion led only to Hex B expression (13). In contrast, in our study both β-hexosaminidase isozymes Hex A and Hex B were generated as a result of a single systemic injection of a mouse transgene-containing scAAV9-Hexb vector. The demonstrated clearance of both GA2 (mainly degraded by Hex B) and GM2 (metabolized by Hex A) suggests that the β-subunit expressed from our vector was not only functional, but also formed αβ heterodimers with endogenous α-monomers. Although the activity levels of these hexosaminidases was not restored to normal, Hex A specifically required for GM2 ganglioside metabolism was increased to around 15% of WT within cerebrum and almost 10% within liver after the therapeutic vector administration. Importantly, given the normal lifespan achieved and lack of disease-associated phenotypes in treated SD mice, this level of enzyme activity is likely to be therapeutic. In fact, the production of even a small percentage

of wild-type activity of these enzymes will probably reach a threshold level sufficient for normal GM2 degradation (37).

The secondary elevation of multiple lysosomal enzymes has been observed in tissues from LSD patients and in some animal models (26, 27), and provides useful biochemical markers of disease burden and therapeutic response. Our data reveal similar secondary enzyme elevations in SD mice, as well as a drastic reduction after scAAV9 vector administration providing further evidence of the efficacy of our approach. In LSDs, accumulation of undegraded material typically increases number and size of lysosomes as evidenced by overexpression of structural lysosomal proteins (38). Our results show that scAAV9-Hexb treatment was efficient in preventing LAMP-1 accumulation, and the expected accumulation of storage material in the brain of SD mutants. *Hexb-/-* mice display significant pathology within the forebrain (7), which also extends to the brainstem and spinal cord. Our data suggest this pathology is especially prominent in the thalamocortical system, and within the cerebellum and brainstem. There appears to be a close association between the distribution of astrocytosis and microglial activation and neuron loss. However, most importantly, we show here that a single intravenous administration was sufficient to prevent this severe neuroinflammation and neuron loss within cerebellum and brainstem, two brain regions that are significantly affected in SD. In summary, we demonstrate in a preclinical model that a single intravenous administration of scAAV9-Hexb vector to newborn *Hexb-/-* mice is effective and sufficient to prevent GM2 ganglioside accumulation in CNS having a long-lasting effect on physical activity, behavior and survival of treated SD mice which are indistinguishable from WT.

MATERIALS AND METHODS

Animals

All animal experiments were carried out in accordance with European guidelines for the care and use of experimental animals. The Sandhoff mouse model was generated by targeted disruption of the *Hexb* gene in the C57BL/6J strain (*Hexb-/-* mice) (5). Wild-type (+/+) C57BL/6J littermates were used as controls in the study. The *Hexb-/-* strain was maintained by two types of breeding: heterozygous females with affected males, and affected females with affected males. To determine the status of newborn mice, total β-hexosaminidase activity was measured from clipped toes using a standard enzymatic assay protocol. Briefly, biopsies were mechanically homogenized in sterile water, incubated on ice for 20 minutes to achieve cell lysis. β-hexosaminidases and β-galactosidase (control enzyme) activities were then measured using the artificial β-*N*-acetylglucosaminide (MUG) and 4-MU-β-D-galactopyranoside substrates, respectively (Sigma). These biochemically determined genotypes were subsequently double-checked by polymerase chain reaction (PCR), as described previously (5). Briefly, samples were incubated at 37°C overnight in urea buffer containing proteinase K (10 mg/ml). Next, phenol was added, followed by 5 minutes centrifugation in order to separate the aqueous phase from the organic phase which was discarded. Subsequently, glycogen (20 mg/ml), ammonium acetate (7.5 M) and pure ethanol were added to the aqueous phase and the solution was incubated at -80°C for 1 hour for DNA precipitation, and DNA was recovered by centrifugation (13000 rpm for 30 min at 4°C). After supernatant removal, 3 washes with 70% ethanol were performed and DNA was resuspended in sterile TE 10:1. The final DNA concentration was evaluated on a Nanodrop (Thermo Scientific). PCR genotyping was performed using three previously described primers (5). PCR samples (50 µl total volume) were preheated at 95°C for 5 min. Forty PCR cycles were performed, composed of 30 s denaturation at 95°C, 30 s annealing at 55°C, and 1 min extension at 72°C. Products were analysed on a 2% agarose gel.

scAAV vector production and *in vivo* administration

Self-complementary genome-containing plasmids were constructed by deleting the D sequence and the terminal resolution site from one of the inverted terminal repeats. The production of serotype 9 AAV has been described elsewhere (14). AAV9 vectors were generated by packaging AAV2-based recombinant self-complementary (sc) genomes into the AAV9 capsids. Virions were produced by transfecting HEK293 cells with (i) the adenovirus helper plasmid (pXX6-80), (ii) the AAV packaging plasmid encoding the *rep2* and the *cap2* or the *cap9* genes, and (iii) the AAV2 shuttle plasmid containing the gene encoding mouse Hexb under the control of the phosphoglycerate kinase (PGK) promoter in the sc genome. Recombinant vectors (rAAV) were purified by double-CsCl ultracentrifugation followed by dialysis against the formulation buffer of the vector stocks, namely phosphate-buffered saline containing 0.5 mM $MgCl_2$ and 1.25 mM KCl (PBS-MK; five buffer changes, 3 hours per round of dialysis). Physical particles were quantified by real-time PCR. Vector titers are expressed as vector genomes per milliliter (vg/ml). Intravenous injections were performed in newborn *Hexb-/-* mice (at day one or two after birth) via the temporal vein (3.5×10^{13} vg/kg in each mouse, volume : 40-60 µl according to the weight, $n = 8$ for survival, $n = 4$ for all other analyses: enzymatic assays, ganglioside analysis, histology).

Behavioral tests

Animals were housed at 25°C during a 12h light/dark cycle, with food and water made available *ad libitum* throughout the experiments. They were first evaluated on physical criteria: weight, general health and tremor. Behavioral tests were carried out on a weekly basis between 11 a.m. and 5 p.m. (except Activmeter). Studies were performed using scAAV9-Hexb treated *Hexb-/-* mice, wild-type and homozygous Sandhoff littermates or age-matched progeny. An accelerating rotarod test was used to evaluate mice motor performance

and coordination. The rotarod (Bioseb) comprises a rotating drum, which speed rises from 4 to 40 rpm over 2 min. The animals (up to 5) were placed on the rotating cylinder to test balance and coordination. The time at which each animal fell from the rod was noted. Each animal did three consecutive trials, the first one was treated as a test and therefore was not considered in the final results. The inverted screen test was used as a measure of grip strength. A single animal was placed onto a clean cage metal grid screen. After placement, the animal was allowed to grip the grid before it was inverted 180° over a plastic cage containing fresh bedding. The latency to fall from the grid was recorded during a 10 second period, after which mice were returned to the home cage.

The righting reflex was analysed to evaluate the muscular strengh of mice. The time taken for animals to right themselves after being lain on their backs within a 10 seconds period was measured. For Activmeter test, single housed animals were recorded over a 10 hour night period (8 p.m. - 6 a.m.) in ages indicated. The cage was placed on an Activmeter platform system (Bioseb) which uses balance system and vibrations within the cage to measure locomotion parameters i.e. distance (cm) and global movement (s). A qualitative analysis of gait was performed by analysing the pattern of footprints made after painting feet different colors. Front and hind mice paws were painted with red and blue ink, respectively and mice were allowed to walk in a tunnel of transparent plexiglas placed on a white sheet of paper (40 cm long) and the footprint was digitalised.

Sample collection and neuropathological analyses

Mice were sacrificed with a lethal dose of 10 $mg.kg^{-1}$ xylazine and 100 mg.kg-^{1} ketamine by intraperitoneal injection. Brain and liver tissues were collected for different analyses. Samples for enzymatic assays and ganglioside analyses were weighted, snap frozen and stored at -80°C until use. Brain tissue used for immunohistochemical analyses was immersed in a freshly

prepared and filtered solution of 4% paraformaldehyde (PFA) in 0.1 M phosphate buffer, pH 7.4 and maintained in PFA for 24h at 4°C. Fixed in PFA brain tissue was bisected along the midline. Single hemispheres were cryoprotected in 30% sucrose, 0.5% sodium azide in 50 mM tris buffered saline (TBS), pH 7.6 prior to sectioning on frozen microtome. 40 m coronal sections through the rostrocaudal extent of the cortical mantle were collected one per well in 96 well plates containing a cryoprotective solution (30% ethylene glycol (Sigma-Aldrich), 15% sucrose, 0.05% sodium azide in TBS (39). All subsequent histological analyses were performed blind to genotype and treatment status.

For direct visualization of neuronal morphology, a series of every sixth section through each brain was slide mounted and Nissl stained with cresyl violet (39). Briefly, slides were incubated in 0.05% cresyl fast violet (Merck), 0.05% acetic acid in water for 30 min at 60°C, rinsed in deionised water, and then differentiated through an ascending series of alcohols before clearing in xylene and coverslipped using DPX mounting medium (VWR).

For immunohistochemistry, a standard protocol was used to examine the distribution of markers of interest (39, 40), using 3,3'-diaminobenzidine tetrahydrochloride (DAB) for visualization. Endogenous peroxidase activity was quenched in 1% hydrogen peroxidase (VWR) in TBS for 15 min. Sections were then rinsed in TBS and blocked in 15% normal serum in TBS with 0.3% Triton-X (TBS-T), before incubation in the appropriate primary antibody; polyclonal rabbit anti-GFAP (Dako, 1:4000), rat anti-CD68 (Serotec, 1:2000), polyclonal rabbit anti-LAMP-1 (Abcam, 1:1000), diluted in 10% normal serum in TBS-T overnight at 4°C. Sections were rinsed in TBS and incubated with the appropriate biotinylated secondary antibodies: swine anti-rabbit (Dako, 1:1000), rabbit anti-rat (Vector, 1:1000) for 2h at room temperature and subsequently rinsed in TBS. They were then incubated in avidin-biotin-peroxidase complex (Vectastain Elite ABC kit, Vector, 1:1000) in TBS for 2h, and rinsed in TBS. To visualize immunoreactivity, sections were incubated in 0.05% DAB

containing 0.001% hydrogen peroxide in TBS for up to 25 min, depending on antigen. Finally, sections were rinsed in ice-cold TBS and then mounted on gelatine-chrome-coated microscope slides (VWR), air-dried overnight, cleared in xylene and coverslipped with DPX (VWR). The quantification of immunohistochemical images was performed using semi-automated thresholding image analysis, as previously described (40, 41). Using a 40x objective, a number of non-overlapping images representing the entire region of interest (30 images for VPM/VPL region and 18 for LGNd) were taken from 3 consecutive sections starting from defined anatomical landmarks (42). *Image Pro Plus* analysis software (Media Cybernetics), was used to determine the area of immunoreactivity for each antigen in each region by applying a threshold that discriminated staining from background in each image. Data were plotted as the mean percentage area of immunoreactivity per field ± SEM for each region.

For neuron cell number estimation, the optical fractionator probe was used (43), in Nissl stained sections of brain regions of interest as described (44, 45). Briefly, Nissl stained cells were counted as neurons if they had clearly identifiable nucleus without considering astrocytes and microglia (cells with small soma). A line was traced around the boundary of the region of interest, a grid was superimposed and cells were counted within a series of dissector frames placed according to the sampling grid size. Different grid and dissector sizes were used in each brain region using a coefficient of error value of less than 0.1 to indicate sampling efficiency (46). For thalamic VPM/VPL region, a 1:6 series was sampled using grid 175 x 175 m and frame 74 x 42 m; for lamina IV of S1BF cortical region a 1:12 series was sampled with grid 150 x 150 m and frame 41 x 26 m; for brainstem regions, a 1:6 section periodicity was used, and the dimensions for the optical fractionator were as follow: DCN - grid: 140 x 140 m, frame: 70 x 40 m; SPV - grid: 270 x 270 m, frame 70 x 40 m.

Enzymatic assays

Brain, brainstem and liver samples (50 mg) were ground in 300 µl of 0.1 M citrate phosphate buffer, pH 4.5 and homogenates were lysed by 3 cycles of rapid freezing and thawing, followed by centrifugation at 4°C for 5 min at 10,000 g. The protein content of each supernatant was determined using the BCA kit (Assay Protein Quantitation Bicinchoninic acid, Pierce) according to the manufacturer's recommendations. Lysosomal enzyme activities (β-galactosidase, β-glucuronidase, α-fucosidase, total β-hexosaminidases and β-hexosaminidase A) were measured in these supernatants (1/10 dilution). In a black 96-well plate with clear bottom: 10 µl of diluted supernatant was added to 50 µl of the fluorimetric corresponding substrate. The samples were incubated for 1 h at 37°C with gentle agitation and enzymatic reactions were stopped by adding 200 µl of a 1M glycine buffer, pH 10. The released fluorescence was read on a CytoFluor 4000 fluorimeter (PerSeptive Biosystems), excitation: 360±40 nm, emission: 460±40 nm. The data obtained were compared with the fluorescence of a 4-methyl-umbelliferone standard (10 nmol/well). Enzyme activities were expressed as nmol/h/mg cell protein. Substrates used were: 4-methylumbelliferyl-β-D-galactopyranoside (Sigma) 1 mM in 0.1M citrate phosphate buffer at pH 4.5 for β-galactosidase, 4-methylumbelliferyl-β-D-glucuronide (Sigma) 1 mM in a 0.1M citrate phosphate buffer at pH 5 for β-glucuronidase, 4-methyl-umbelliferyl-α-L-fucopyranoside (Sigma) 1 mM in 0.1M citrate phosphate buffer at pH 4.5 for α-fucosidase, 4-methylumbelliferyl-2-acetamido-2-deoxy-β-D-glucopyranoside (Sigma) (MUG) 1 mM in 0.1M citrate phosphate buffer at pH 4.5 for total β-hexosaminidases, 4-methylumbelliferyl-7-(6-sulfo-2-acetamido-2-deoxy-β-D-glucopyranoside (MUGS) (Calbiochem) 1 mM in 0.1M citrate phosphate buffer at pH 4.5 for β-hexosaminidase A, 4-methylumbelliferone (Sigma) 1 mM in deionized water for standard.

Biochemical analysis of gangliosides and other glycosphingolipids

Analyses were performed on frozen cerebral hemispheres and dissected cerebellae which had been stored at -80°C prior to use. Total lipid extraction, separation and purification of main lipid fractions were done using previously described procedures (47, 48). Briefly, total lipids were extracted from 20% tissue homogenates in water using chloroform-methanol 1:2 (v/v). For ganglioside studies, part of the extract (corresponding to 20-50 mg tissue) was desalted and separated into two fractions on reverse-phase 100 mg Bond Elut C18 columns (Varian) using a downscaling of a published procedure (49). The methanol-water 12:1 (v/v) eluate containing all the gangliosides was used without further purification. An aliquot corresponding to 1.5 or 3 mg of tissue was spotted (Linomat 5 device, Camag) on silica gel 60 high-performance thin layer chromatography (HPTLC) plates (Merck). Plates were developed in chloroform–methanol–0.2% $CaCl_2$ 55:45:10 (v/v/v) and sprayed with resorcinol-HCl reagent to visualize the sialic acid moiety of individual gangliosides. Densitometric quantification was performed at 580 nm (Camag TLCII scanner, Cats software). The data were normalized to the number of sialic acids per individual ganglioside and expressed as % of total gangliosides. For gangliotriaosylceramide (GA2) studies, part of the total lipid extract was saponified, desalted by phase partition, and suitable aliquots were spotted on HPTLC plates. After development in chloroform–methanol–water 65:25:4 (v/v/v), hexose-containing compounds were visualized by orcinol-sulphuric acid reagent and densitometric quantification was performed.

Statistical analysis

Microsoft Excel (Redmond) was used for data collection and for statistical analysis and graph representation was conducted using *GraphPad Prism Version 6* for Mac (GraphPad Software). To test for significance between groups, the Student's t-test or ANOVA test with

post hoc Bonferroni analysis were used as appropriate. All graphs are plotted as the mean ± the standard error of the mean (SEM).

ACKNOWLEDGEMENTS

We are grateful to the members of INSERM U1151 for support. We thank personnel of SFR Animal Facility for excellent technical support. We thank the Vector Core of the University Hospital of Nantes supported by the *Association Française contre les Myopathies* (AFM) for providing the AAV vectors. N.N. received a doctoral fellowship from the *Association Française contre les Myopathies* (AFM) and the association *Vaincre les Maladies Lysosomales* (VML). L.R. received a doctoral fellowship from the association *Vaincre les Maladies Lysosomales* (VML). The work was supported by a grant from the *Association Française contre les Myopathies* (AFM) and the association *Vaincre les Maladies Lysosomales* (VML) to C.C.

CONFLICT OF INTEREST STATEMENT

The authors have no conflict of interest.

REFERENCES

1. Sandhoff, K., Harzer, K., Wässle, W. and Jatzkewitz, H. (1971) Enzyme alterations and lipid storage in three variants of Tay-Sachs disease. *J. Neurochem.*, **18**, 2469–2489.
2. Gravel, R.A., Kaback, M.M., Proia, R.L., Sandhoff, K., Suzuki, K. and Suzuki, K. (2001) The GM2 gangliosidoses. In Scriver C.R., Beaudet A.L., Sly W.S., Valle D. (ed.), *Metabolic and Molecular Bases of Inherited Disease.* McGraw-Hill, New York, USA, Vol. 3, pp. 3827–3876.
3. Neufeld, E.F. (1989) Natural history and inherited disorders of a lysosomal enzyme, beta-hexosaminidase. *J. Biol. Chem.*, **264**, 10927–10930.
4. Sango, K., Yamanaka, S., Hoffmann, A., Okuda, Y., Grinberg, A., Westphal, H., McDonald, M.P., Crawley, J.N., Sandhoff, K., Suzuki, K., *et al.* (1995) Mouse models of Tay–Sachs and Sandhoff diseases differ in neurologic phenotype and ganglioside metabolism. *Nat. Genet.*, **11**, 170–176.
5. Phaneuf, D., Wakamatsu, N., Huang, J.-Q., Borowski, A., Peterson, A.C., Fortunato, S.R., Ritter, G., Igdoura, S.A., Morales, C.R., Benoit, G., *et al.* (1996) Dramatically

different phenotypes in mouse models of human Tay-Sachs and Sandhoff diseases. *Hum. Mol. Genet.*, **5**, 1–14.
6. Huang, J.-Q., Trasler, J.M., Igdoura, S., Michaud, J., Hanai, N. and Gravel, R.A. (1997) Apoptotic cell death in mouse models of GM2 gangliosidosis and observations on human Tay-Sachs and Sandhoff diseases. *Hum. Mol. Genet.*, **6**, 1879–1885.
7. Wada, R., Tifft, C.J. and Proia, R.L. (2000) Microglial activation precedes acute neurodegeneration in Sandhoff disease and is suppressed by bone marrow transplantation. *Proc. Natl. Acad. Sci. USA*, **97**, 10954–10959.
8. Jeyakumar, M., Thomas, R., Elliot-Smith, E., Smith, D.A., Spoel, V.D., C,A., d'Azzo, A., Hugh Perry, V., Butters, T.D., Dwek, R.A., *et al.* (2003) Central nervous system inflammation is a hallmark of pathogenesis in mouse models of GM1 and GM2 gangliosidosis. *Brain*, **126**, 974–987.
9. Matsuoka, K., Tamura, T., Tsuji, D., Dohzono, Y., Kitakaze, K., Ohno, K., Saito, S., Sakuraba, H. and Itoh, K. (2011) Therapeutic potential of intracerebroventricular replacement of modified human β-hexosaminidase B for GM2 gangliosidosis. *Mol. Ther.*, **19**, 1017–1024.
10. Maegawa, G.H.B., Tropak, M., Butner, J., Stockley, T., Kok, F., Clarke, J.T.R. and Mahuran, D.J. (2007) Pyrimethamine as a potential pharmacological chaperone for late-onset forms of gm2 gangliosidosis. *J. Biol. Chem.*, **282**, 9150–9161.
11. Jeyakumar, M., Smith, D.A., Williams, I.M., Borja, M.C., Neville, D.C.A., Butters, T.D., Dwek, R.A. and Platt, F.M. (2004) NSAIDs increase survival in the Sandhoff disease mouse: Synergy with N-butyldeoxynojirimycin. *Ann. Neurol.*, **56**, 642–649.
12. Cachón-González, M.B., Wang, S.Z., Lynch, A., Ziegler, R., Cheng, S.H. and Cox, T.M. (2006) Effective gene therapy in an authentic model of Tay-Sachs-related diseases. *Proc. Natl. Acad. Sci. USA*, **103**, 10373–10378.
13. Cachón-González, M.B., Wang, S.Z., McNair, R., Bradley, J., Lunn, D., Ziegler, R., Cheng, S.H. and Cox, T.M. (2012) Gene transfer corrects acute GM2 gangliosidosis—potential therapeutic contribution of perivascular enzyme flow. *Mol. Ther.*, **20**, 1489–1500.
14. Duque, S., Joussemet, B., Riviere, C., Marais, T., Dubreil, L., Douar, A.-M., Fyfe, J., Moullier, P., Colle, M.-A. and Barkats, M. (2009) Intravenous administration of self-complementary AAV9 enables transgene delivery to adult motor neurons. *Mol. Ther.*, **17**, 1187–1196.
15. Foust, K.D., Nurre, E., Montgomery, C.L., Hernandez, A., Chan, C.M. and Kaspar, B.K. (2009) Intravascular AAV9 preferentially targets neonatal-neurons and adult-astrocytes in CNS. *Nat. Biotechnol.*, **27**, 59–65.
16. Valori, C.F., Ning, K., Wyles, M., Mead, R.J., Grierson, A.J., Shaw, P.J. and Azzouz, M. (2010) Systemic delivery of scAAV9 expressing SMN prolongs survival in a model of spinal muscular atrophy. *Sci. Transl. Med.*, **2**, 35–42.
17. Foust, K.D., Wang, X., McGovern, V.L., Braun, L., Bevan, A.K., Haidet, A.M., Le, T.T., Morales, P.R., Rich, M.M., Burghes, A.H.M., *et al.* (2010) Rescue of the spinal muscular atrophy phenotype in a mouse model by early postnatal delivery of SMN. *Nat. Biotechnol.*, **28**, 271–274.
18. Dominguez, E., Marais, T., Chatauret, N., Benkhelifa-Ziyyat, S., Duque, S., Ravassard, P., Carcenac, R., Astord, S., Pereira de Moura, A., Voit, T., *et al.* (2011) Intravenous scAAV9 delivery of a codon-optimized SMN1 sequence rescues SMA mice. *Hum. Mol. Genet.*, **20**, 681–693.
19. Fu, H., Dirosario, J., Killedar, S., Zaraspe, K. and McCarty, D.M. (2011) Correction of neurological disease of mucopolysaccharidosis IIIB in adult mice by rAAV9 trans-blood-brain barrier gene delivery. *Mol. Ther.*, **19**, 1025–1033.

20. Haurigot, V., Marcó, S., Ribera, A., Garcia, M., Ruzo, A., Villacampa, P., Ayuso, E., Añor, S., Andaluz, A., Pineda, M., *et al.* (2013) Whole body correction of mucopolysaccharidosis IIIA by intracerebrospinal fluid gene therapy. *J. Clin. Invest.*, **128**, 3254–3271.
21. Ruzo, A., Marcó, S., García, M., Villacampa, P., Ribera, A., Ayuso, E., Maggioni, L., Mingozzi, F., Haurigot, V. and Bosch, F. (2012) Correction of pathological accumulation of glycosaminoglycans in central nervous system and peripheral tissues of MPSIIIA mice through systemic AAV9 gene transfer. *Hum. Gene Ther.*, **23**, 1237–1246.
22. Weismann, C.M., Ferreira, J., Keeler, A.M., Su, Q., Qui, L., Shaffer, S.A., Xu, Z., Gao, G. and Sena-Esteves, M. (2015) Systemic AAV9 gene transfer in adult GM1 gangliosidosis mice reduces lysosomal storage in CNS and extends lifespan. *Hum. Mol. Genet.*, **24**, 4353–4364.
23. Inagaki, K., Fuess, S., Storm, T.A., Gibson, G.A., Mctiernan, C.F., Kay, M.A. and Nakai, H. (2006) Robust systemic transduction with AAV9 vectors in mice: efficient global cardiac gene transfer superior to that of AAV8. *Mol. Ther.*, **14**, 45–53.
24. Walia, J.S., Altaleb, N., Bello, A., Kruck, C., LaFave, M.C., Varshney, G.K., Burgess, S.M., Chowdhury, B., Hurlbut, D., Hemming, R., *et al.* (2015) Long-term correction of Sandhoff disease following intravenous delivery of rAAV9 to mouse neonates. *Mol. Ther.*, **23**, 414–422.
25. Osmon, K.J.L., Woodley, E., Thompson, P., Ong, K., Karumuthil-Melethil, S., Keimel, J.G., Mark, B.L., Mahuran, D., Gray, S.J. and Walia, J.S. (2016) Systemic gene transfer of a hexosaminidase variant using an scAAV9.47 vector corrects GM2 gangliosidosis in Sandhoff mice. *Hum. Gene Ther.*, **27**, 497–508.
26. Sands, M.S., Vogler, C., Torrey, A., Levy, B., Gwynn, B., Grubb, J., Sly, W.S. and Birkenmeier, E.H. (1997) Murine mucopolysaccharidosis type VII: long term therapeutic effects of enzyme replacement and enzyme replacement followed by bone marrow transplantation. *J. Clin. Invest.*, **99**, 1596–1605.
27. Vogler, C., Galvin, N., Levy, B., Grubb, J., Jiang, J., Zhou, X.Y. and Sly, W.S. (2003) Transgene produces massive overexpression of human β-glucuronidase in mice, lysosomal storage of enzyme, and strain-dependent tumors. *Proc. Natl. Acad. Sci. USA*, **100**, 2669–2673.
28. Ribera, A., Haurigot, V., Garcia, M., Marcó, S., Motas, S., Villacampa, P., Maggioni, L., León, X., Molas, M., Sánchez, V., *et al.* (2015) Biochemical, histological and functional correction of mucopolysaccharidosis Type IIIB by intra-cerebrospinal fluid gene therapy. *Hum. Mol. Genet.*, **24**, 2078–2095.
29. Motas, S., Haurigot, V., Garcia, M., Marcó, S., Ribera, A., Roca, C., Sánchez, X., Sánchez, V., Molas, M., Bertolin, J., *et al.* (2016) CNS-directed gene therapy for the treatment of neurologic and somatic mucopolysaccharidosis type II (Hunter syndrome). *JCI Insight*, **1**, e86696.
30. Sands, M.S. and Davidson, B.L. (2006) Gene therapy for lysosomal storage diseases. *Mol. Ther.*, **13**, 839–849.
31. Clancy, B., Finlay, B.L., Darlington, R.B. and Anand, K.J.S. (2007) Extrapolating brain development from experimental species to humans. *NeuroToxicology*, **28**, 931–937.
32. Workman, A.D., Charvet, C.J., Clancy, B., Darlington, R.B. and Finlay, B.L. (2013) Modeling transformations of neurodevelopmental sequences across mammalian species. *J. Neurosci.*, **33**, 7368–7383.
33. Tanguy, Y., Biferi, M.G., Besse, A., Astord, S., Cohen-Tannoudji, M., Marais, T. and Barkats, M. (2015) Systemic AAVrh10 provides higher transgene expression than AAV9 in the brain and the spinal cord of neonatal mice. *Front. Mol. Neurosci.*, **8:36**.

34. Gray, S.J., Matagne, V., Bachaboina, L., Yadav, S., Ojeda, S.R. and Samulski, R.J. (2011) Preclinical differences of intravascular AAV9 delivery to neurons and glia: a comparative study of adult mice and nonhuman primates. *Mol. Ther.*, **19**, 1058–1069.
35. Forsayeth, J.R. and Bankiewicz, K.S. (2011) AAV9: over the fence and into the woods. *Mol. Ther.*, **19**, 1006–1007.
36. Chandler, R.J., LaFave, M.C., Varshney, G.K., Burgess, S.M. and Venditti, C.P. (2016) Genotoxicity in mice following AAV gene delivery: a safety concern for human gene therapy? *Mol. Ther.*, **24**, 198–201.
37. Conzelmann, E., Kytzia, H.J., Navon, R. and Sandhoff, K. (1983) Ganglioside GM2 N-acetyl-beta-D-galactosaminidase activity in cultured fibroblasts of late-infantile and adult GM2 gangliosidosis patients and of healthy probands with low hexosaminidase level. *Am. J. Hum. Genet.*, **35**, 900–913.
38. Meikle, P.J., Brooks, D.A., Ravenscroft, E.M., Yan, M., Williams, R.E., Jaunzems, A.E., Chataway, T.K., Karageorgos, L.E., Davey, R.C., Boulter, C.D., *et al.* (1997) Diagnosis of lysosomal storage disorders: evaluation of lysosome-associated membrane protein LAMP-1 as a diagnostic marker. *Clin. Chem.*, **43**, 1325–1335.
39. Bible, E., Gupta, P., Hofmann, S.L. and Cooper, J.D. (2004) Regional and cellular neuropathology in the palmitoyl protein thioesterase-1 null mutant mouse model of infantile neuronal ceroid lipofuscinosis. *Neurobiol. Dis.*, **16**, 346–359.
40. Pontikis, C.C., Cella, C.V., Parihar, N., Lim, M.J., Chakrabarti, S., Mitchison, H.M., Mobley, W.C., Rezaie, P., Pearce, D.A. and Cooper, J.D. (2004) Late onset neurodegeneration in the Cln3-/- mouse model of juvenile neuronal ceroid lipofuscinosis is preceded by low level glial activation. *Brain Res.*, **1023**, 231–242.
41. Pontikis, C.C., Cotman, S.L., MacDonald, M.E. and Cooper, J.D. (2005) Thalamocortical neuron loss and localized astrocytosis in the Cln3Deltaex7/8 knock-in mouse model of Batten disease. *Neurobiol. Dis.*, **20**, 823–836.
42. Paxinos, G. and Franklin, B. (2001) *The Mouse Brain in Stereotaxic Coordinates*. Academic press, San Diego, CA.
43. West, M.J., Slomianka, L. and Gundersen, H.J. (1991) Unbiased stereological estimation of the total number of neurons in the subdivisions of the rat hippocampus using the optical fractionator. *Anat. Rec.*, **231**, 482–497.
44. Kielar, C., Maddox, L., Bible, E., Pontikis, C.C., Macauley, S.L., Griffey, M.A., Wong, M., Sands, M.S. and Cooper, J.D. (2007) Successive neuron loss in the thalamus and cortex in a mouse model of infantile neuronal ceroid lipofuscinosis. *Neurobiol. Dis.*, **25**, 150–162.
45. Pressey, S.N.R., O'Donnell, K.J., Stauber, T., Fuhrmann, J.C., Tyynelä, J., Jentsch, T.J. and Cooper, J.D. (2010) Distinct neuropathologic phenotypes after disrupting the chloride transport proteins ClC-6 or ClC-7/Ostm1. *J. Neuropathol. Exp. Neurol.*, **69**, 1228–1246.
46. Gundersen, H.J., Jensen, E.B., Kiêu, K. and Nielsen J., (1999) The efficiency of systematic sampling in stereology--reconsidered. *J. Microsc.*, **193**, 199–211.
47. Fujita, N., Suzuki, K., Vanier, M.T., Popko, B., Maeda, N., Klein, A., Henseler, M., Sandhoff, K., Nakayasu, H. and Suzuki, K. (1996) Targeted disruption of the mouse sphingolipid activator protein gene: a complex phenotype, including severe leukodystrophy and wide-spread storage of multiple sphingolipids. *Hum. Mol. Genet.*, **5**, 711–725.
48. Reid, P.C., Lin, S., Vanier, M.T., Ohno-Iwashita, Y., Harwood, H.J., Hickey, W.F., Chang, C.C.Y. and Chang, T.-Y. (2008) Partial blockage of sterol biosynthesis with a squalene synthase inhibitor in early postnatal Niemann-Pick type C npcnih null mice brains reduces neuronal cholesterol accumulation, abrogates astrogliosis, but may inhibit myelin maturation. *J. Neurosci. Methods*, **168**, 15–25.

49. Kyrklund, T. (1987) Two procedures to remove polar contaminants from a crude brain lipid extract by using prepacked reversed-phase columns. *Lipids*, **22**, 274–277.

LEGENDS TO FIGURES

Figure 1: Partial restoration of hexosaminidases activities in brain, brainstem and liver of scAAV9-treated animals at 2 and 4 months

Enzymatic assays were performed by using the synthetic substrates MUG (4-methylumbelliferyl-2-acetamido-2-deoxy-β-D-glucopyranoside) and MUGS (4-methylumbelliferyl-7-(6-sulfo-2-acetamido-2-deoxy-β-D-glucopyranoside)) to measure either total hexosaminidases activity (A,C,E) or hexosaminidase A specific activity (B,D,F), respectively. Total hexosaminidases and hexosaminidase A activities are presented as percentage of wild-type (WT). Error bars show SEM, n =3-4, *p<0.05, **p<0.01,*** p<0.001, **** p<0.0001 using one way ANOVA.

Figure 2: Reduction of secondary elevation of lysosomal enzymes and storage after the scAAV9-Hexb treatment

Brain (A) and brainstem (B) of WT, *Hexb-/-* and scAAV9-treated mice at 2 and 4 months were tested for β-glucuronidase, α-fucosidase and β-galactosidase activities. Enzymatic activities are presented as percentage of WT for each enzyme. Error bars show SEM, n =3-4, *p<0.05, **p<0.01, *** p<0.001, **** p<0.0001 using one way ANOVA. (C) Brain sections were Nissl stained with cresyl fast violet. An abnormal swollen morphology of neuron cell bodies (arrows) can be observed in the thalamus of 4 months old *Hexb-/-* mice. This appearance was no longer evident in scAAV9-treated animals, which showed a neuronal morphology similar to WT. Scale bars: 50 μm. (D) Brain section of 4 month-old *Hexb-/-* animals shows a huge accumulation of LAMP-1 immunoreactivity by comparison with WT and scAAV9-treated mice. A higher magnification of S1BF lamina IV shows dense

concentration of punctate LAMP-1 staining within all cells in untreated SD mice, but not in scAAV9-treated and WT mice. Scale bars: full sections : 500 μm; higher magnification : 100 μm.

Figure 3: HPTLC analysis of gangliosides and glycosphingolipids within cerebrum and cerebellum of 2 and 4 month-old WT, *Hexb-/-* and scAAV9-treated mice

Gangliosides (A,B) and other glycosphingolipids (C) were studied in cerebrum and cerebellum of 2 and 4 month-old wild type, naive *Hexb-/-* and scAAV9-treated mice. (A) Chromatographic profiles of total gangliosides (resorcinol-HCl staining), showing a drastic and selective reduction of the GM2 ganglioside accumulation in scAAV9-treated mice, compared to the massive storage observed in age-matched untreated SD mice. Each lane corresponds to 3 mg wet weight tissue. (B) Quantitative data for GM2 ganglioside (expressed as percentage of total gangliosides) in cerebrum and cerebellum. (C) Other glycosphingolipids (2 mg tissue/lane), separated on HPTLC plates and visualized by orcinol-sulfuric reagent. A huge accumulation of GA2 is noticeable in SD mice by comparison with WT and scAAV9-treated mice. Gal-Cer, galactosylceramide; GA2, gangliotriaosylceramide.

Figure 4: Prevention of astrocytosis in the thalamocortical system following the IV administration of scAAV9-Hexb vector

(A) Nissl stained section indicating the brain regions analyzed: somatosensory barrelfield cortex (S1BF), dorsal lateral geniculate nucleus (LGNd) and ventral posteromedial/posterolateral nuclei (VPM/VPL**).** (B,D) GFAP immunostaining revealed the extent of astrocytosis within the thalamus (B) and cortex (D) of WT, *Hexb-/-* and scAAV9-treated animals at 2 and 4 months. Astrocytosis was already present as more intensely stained astrocytes at 2 months, and increased with time in thalamus (B) and cortex (D), as was

associated with astrocyte hypertrophy (see inserts). However, astrocytosis was virtually absent in WT and scAAV9 mice in both regions. (C,E) Quantification of GFAP immunoreactivity shows a significant reduction of astrocytosis in 4 months scAAV9-treated mice in thalamus and cortex. Error bars show SEM, n = 3-4, *** $p<0.001$, **** $p<0.0001$ using one way ANOVA.

Figure 5: Prevention of microgliosis and neuronal loss in the thalamocortical system after scAAV9-Hexb treatment

CD68 immunostained sections from WT, *Hexb-/-* and scAAV9-treated animals reveal the different extents of microglial activation at 2 and 4 months of age. The thalamus (A) and cortex (C) of WT controls and scAAV9 treated animals show very few and more palely stained microglia with a small cell soma, whereas the *Hexb-/-* mice displayed a robust and progressive microgliosis throughout brain (A,C), which was especially pronounced in the VPM/VPL. Quantification of CD68 immunoreactivity (B,D) showed significant less microglial activation at 2 months in scAAV9-treated animals, and this treatment effect was maintained at 4 months of age in both thalamus and cortex. (E) Unbiased stereological counts of Nissl stained neuron number in the thalamocortical system of 4 months old scAAV9 treated mice revealed the near complete prevention of this vulnerable neuron population. Error bars show SEM, n = 3-4, *** $p<0.001$, **** $p<0.0001$ using one way ANOVA. Scale bar: thalamus 500 μm, insert 50 μm; cortex 100 μm, insert 50 μm.

Figure 6: Prevention of astrocytosis in brainstem after scAAV9-Hexb treatment

(A) Nissl stained section indicating brain regions analyzed: Cb-Cerebellum; Bs-Brainstem; RF-reticular formation; SPV-spinal trigeminal nucleus V; DCN-deep cerebral nuclei. Higher magnification: cerebellar layers: ML-molecular layer; GL-granular layer; WM-white matter.

(B,D) GFAP immunostaining was performed on brainstem sections of WT, *Hexb-/-* and scAAV9-treated animals at 2 and 4 months revealing astrocytosis within SPV (B) and RF (D) regions in SD mice. Astrocytosis was virtually absent in WT and scAAV9 mice in both regions. (C,E) Quantitative thresholding image analysis of GFAP immunoreactivity in brainstem of *Hexb-/-* mice show consistent upregulation of this marker at 2 and 4 months compared to age-matched controls. scAAV9-treated mice show absence of astrocytosis in the SPV (C) and RF (E) regions of brainstem. This expression is comparable to WT littermates. Error bars show SEM, n = 3-4, *p<0.05, **p<0.01, ***p<0.001, ****p<0.0001 using one-way ANOVA. Scale bar: 50 μm.

Figure 7: Significant correction of microglial activation and neuronal loss prevention in brainstem and cerebellum of treated mice

(A,B) CD68 immunostained sections from WT, *Hexb-/-* and scAAV9-treated animals reveal microglial activation at 2 and 4 months of age in different regions of brainstem. The SPV (A) and RF (B) regions of WT and scAAV9 treated animals show a more palely stained microglia, whereas the *Hexb-/-* mice displayed a robust microgliosis. Quantitative thresholding image analysis of CD68 expression within SPV (C) and RF (D) revealed increased CD68 expression in *Hexb-/-* mice and no significant microgliosis in WT and scAAV9-treated mice. (E,F) Unbiased optical fractionator estimates of the number of Nissl-stained neurons in brainstem and cerebellum of *Hexb-/-*, WT and scAAV9-treated mice revealed a significant loss of neurons within spinal nucleus of the trigeminal nerve SPV (E) and deep cerebellar nuclei DCN (F) in SD mice. At the age of 4 months, total prevention of this loss of neurons was found in the corresponding regions of scAAV9-Hexb samples. Error bars show SEM, n = 3-4, *p<0.05, **p<0.01, ***p<0.001, ****p<0.0001 using one-way ANOVA. Scale bar: 50 μm.

Figure 8: Life expectancy was prolonged, body weight maintained and behavioral performance improved in AAV9-treated mice

(A) Kaplan-Meier survival curve is shown for WT (n = 7), low dose scAAV9 (n = 6), high dose scAAV9 treated (n = 8) and untreated *Hexb-/-* (n = 8) mice. Animals treated with 3.5 x 10^{13} vg/kg reached > 700 days, while untreated Sandhoff mice died around 120 days. (B) Weight was evaluated each week in the different groups of mice. The body weight was maintained in mice treated with scAAV9-Hexb vector (curve comparable to WT group). (C) Mice were subjected to inverted screen test. Latency to fall from metal grid within 10 s test decreases progressively in untreated *Hexb-/-* mice, whereas mutant mice treated with 3.5 x 10^{13} vg/kg scAAV9-Hexb obtain results identical to WT controls throughout entire experiment. (D) WT, *Hexb-/-* and scAAV9-Hexb treated SD mice were tested using an accelerating rotarod. They were put on the accelerating cylinder and the length of time mice stayed on the rod before falling was recorded. A decline of the ability to stay on rotarod was progressively observed in SD mice while results were similar between WT and scAAV9-treated animals until 700 days.

SUPPLEMENTARY INFORMATION

Video S1: The video shows a scAAV9-Hexb treated mouse and a WT mouse (aged 23 months) in their home-cage environment. Mice are both active and they are undistinguishable from each other.

Figure S1: Prevention of lysosomal storage in hypothalamus, cortex, and hippocampus

LAMP-1 immunostained brain sections from 4 months-old *Hexb-/-* animals show a huge accumulation of this lysosomal marker at multiple rostrocaudal levels of the hypothalamus, cortex, and hippocampus. No upregulation of LAMP-1 can be observed in WT or in scAAV9-treated samples. Scale bars: 500 μm.

Figure S2: Reduction of neuroinflammation in LGNd thalamic region in scAAV9-treated mice

(A) Astrocytosis was prevented in scAAV9-treated SD mice by comparison with untreated *Hexb-/-* mice, which showed a significant increase in GFAP immunoreactivity at 4 months. (B) Microgliosis was similarly dramatically less in scAAV9-treated mice at 4 months in comparison with untreated *Hexb-/-* mice showing a huge immunoreactivity at 4 months. Error bars show SEM, n = 3-4, *p<0.05, **p<0.01, ***p<0.001, ****p<0.0001 using one way ANOVA.

Figure S3: Correction of astrocytosis in cerebellum following IV administration of scAAV9-Hexb vector

GFAP-immunostaining on cerebellum sections reveals the extent of astrocytosis in WT, untreated *Hexb-/-* and scAAV9-treated animals at 2 and 4 months. (A) DCN (B) molecular layer (E) granular layer (F) white matter. Intensely stained astrocytes were present at 2 and 4 months in SD mice, but astrocytosis was prevented/reduced in scAAV9-treated mice. Results were confirmed by the quantitative thresholding image analyses (C,D,G,H). Error bars show SEM, n = 3-4, *p<0.05, **p<0.01, ***p<0.001, ****p<0.0001 using one way ANOVA. Scale bar: 50 μm.

Figure S4: Significant correction of microglial activation in cerebellum in treated mice

CD68-immunostaining was performed on cerebellum sections to evaluate microglial activation in WT, *Hexb-/-* and scAAV9-treated animals at 2 and 4 months. (A) DCN (B) molecular layer (E) granular layer (F) white matter. Microglial activation was nearly absent in scAAV9-treated mice by comparison with untreated mice. Results were confirmed by the quantitative thresholding image analyses (C,D,G,H). SEM, n = 3-4, *p<0.05, **p<0.01, ***p<0.001, ****p<0.0001 using one way ANOVA. Scale bar: 50 μm.

Figure S5: Qualitative gait analysis reveals absence of ataxic pattern in scAAV9-treated mice

Gait was analysed via a footprint test performed in WT, untreated *Hexb*-/- and scAAV9-treated mutant mice (4, 12, 16 and 20 months). While untreated *Hexb*-/- mice displayed a markedly abnormal gait with dragging of the hindlimbs at 4 months, scAAV9-Hexb animals showed no such gait aberrations even at 20 months.

Figure S6: Correction of behavioral deficits following intravenous scAAV9-Hexb delivery

(A) Activmeter acquisition during a 10h night period showed hyperactivity of untreated *Hexb*-/- mice compared to WT at 2 months, and subsequent drastic decline at 4 months. Total movement was not significantly different between scAAV9-treated and WT mice at different time points from 2 to 20 months, except during the late period (mean ± SEM of $n = 3$ per group). (B) No significant difference was found for the total distance covered between scAAV9-treated and WT mice at 12 months (error bars show SEM, $n = 3$-4, $p>0.5$, t-test).

ABBREVIATIONS

Bs : brainstem

Cb : cerebellum

cDNA : complementary DNA

CNS : central nervous system

DCN : dorsal cochlear nucleus

GFAP : glial fibrillary acidic protein

GL : granular layer

GA2 : gangliotriaosylceramide

HPTLC : high-performance thin layer chromatography

LGNd : dorsal lateral geniculate nucleus

LSD : lysosomal storage disorder

ML : molecular layer

MU : methylumbelliferyl

PGK : phosphoglycerate kinase

RF : reticular formation

scAAV9 : self complementary adeno-associated virus

S1BF : somatosensory barrelfield cortex

SD : Sandhoff disease

SPV : spinal trigeminal nucleus V

TBS : tris buffered saline

vg : vector genome

VPM : ventral posteromedial nuclei

VPL : ventral posterolateral nuclei

WM : white matter

WT : wild-type

Figure 1

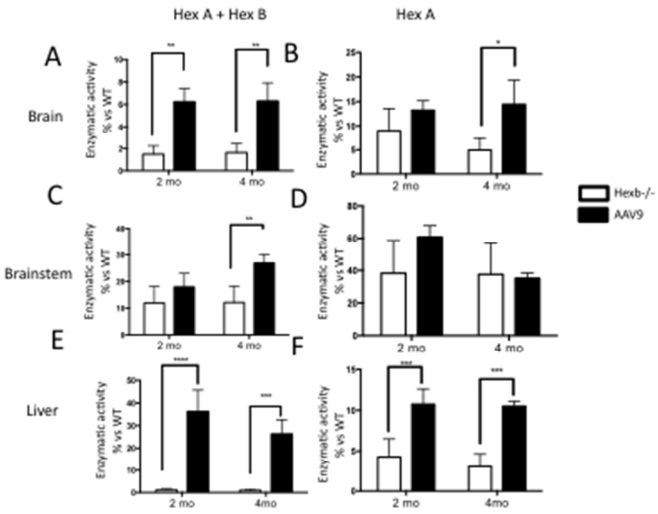

Figure 1

190x254mm (72 x 72 DPI)

Figure 2

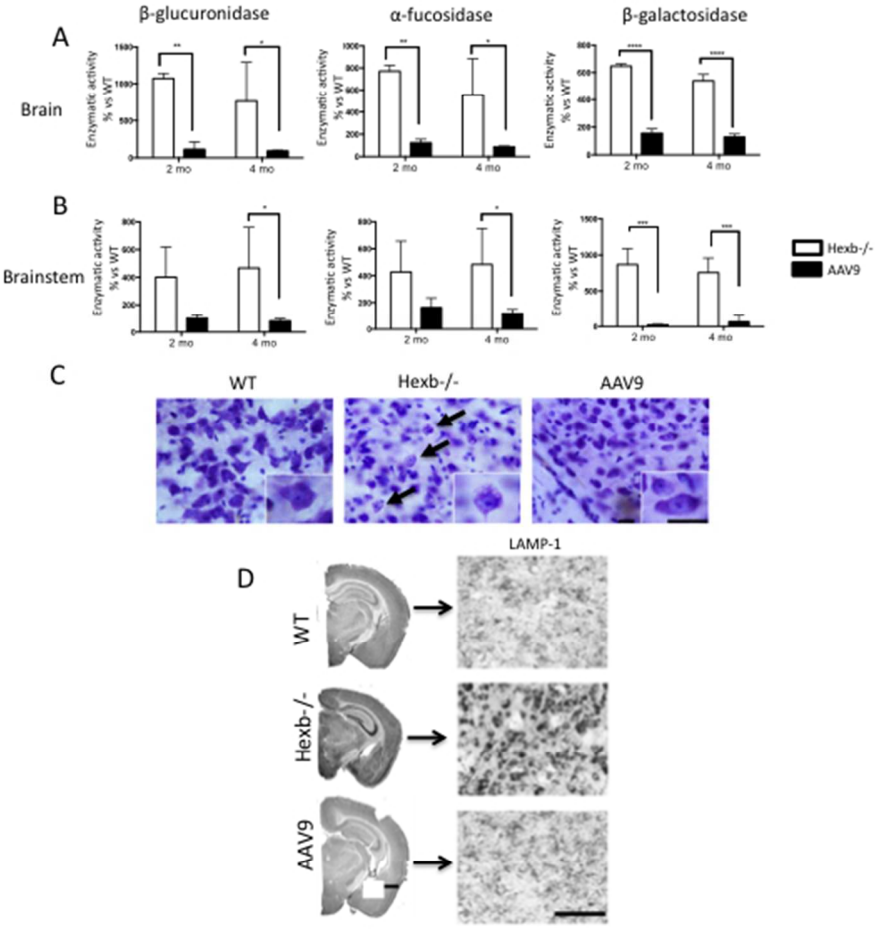

Figure 2

190x254mm (72 x 72 DPI)

Figure 3

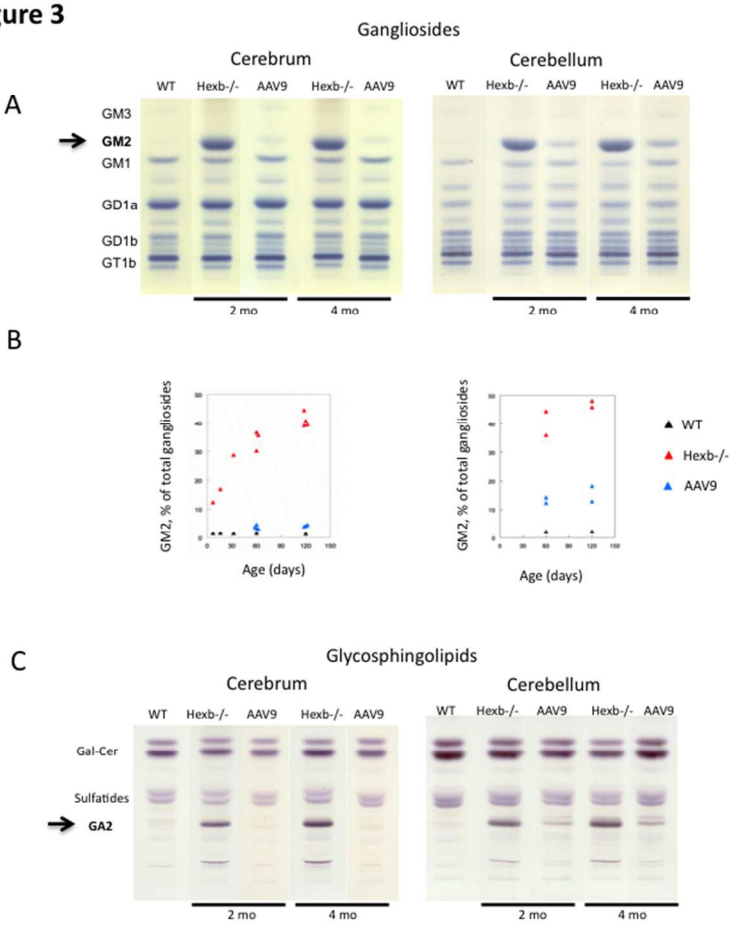

Figure 3

264x352mm (72 x 72 DPI)

Figure 4

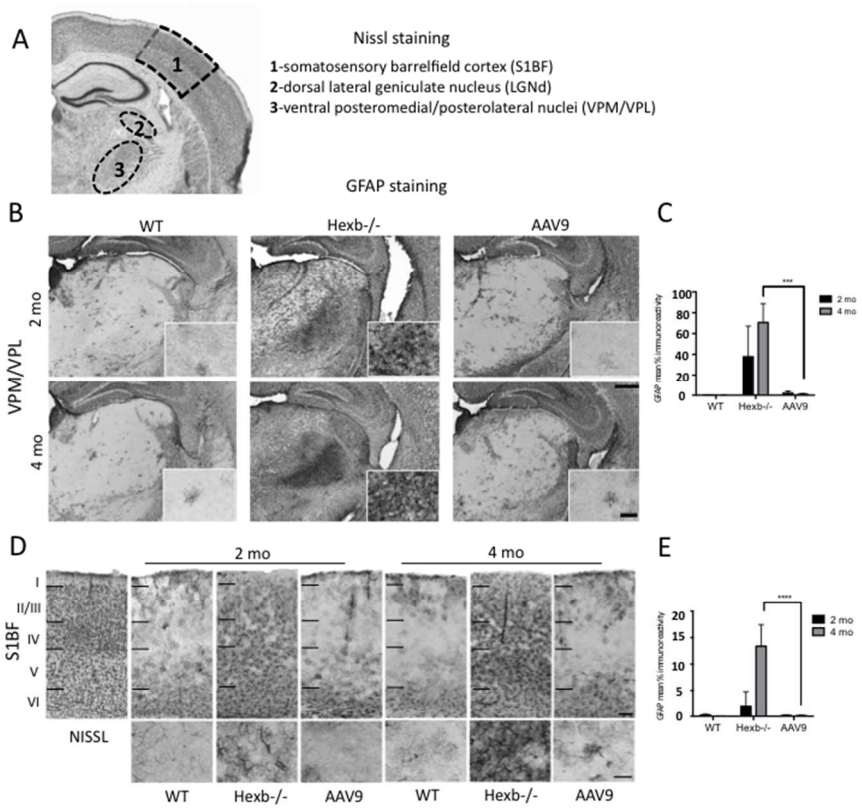

Figure 4

264x352mm (72 x 72 DPI)

Figure 5

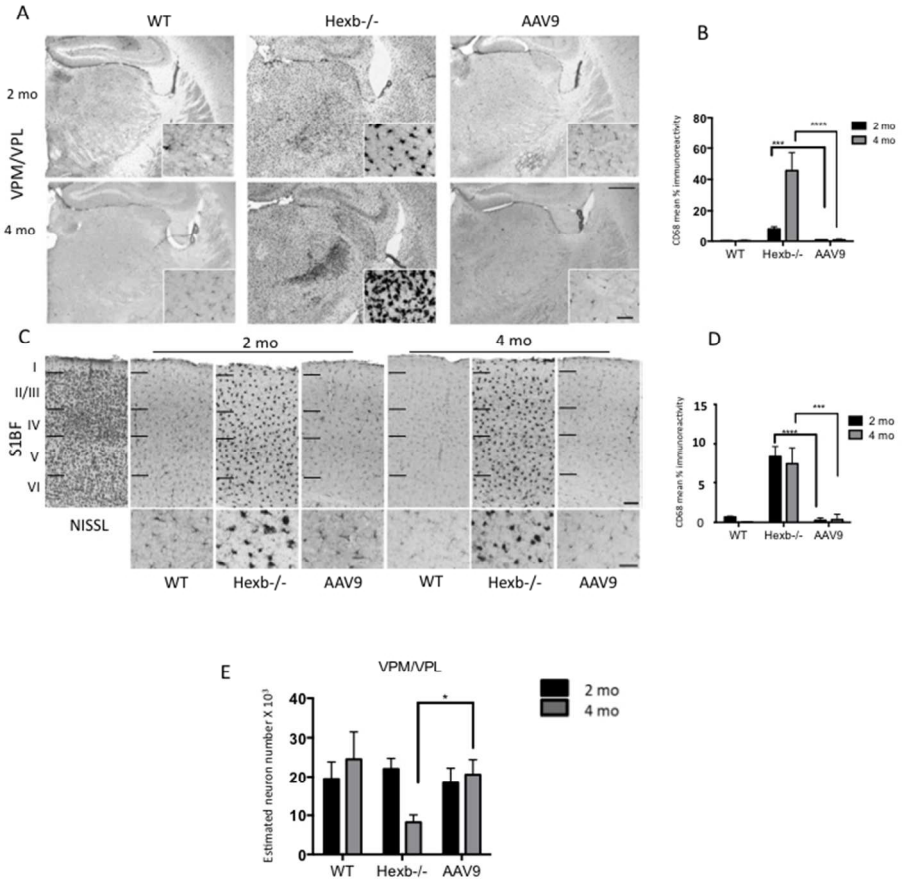

Figure 5

264x352mm (72 x 72 DPI)

Figure 6

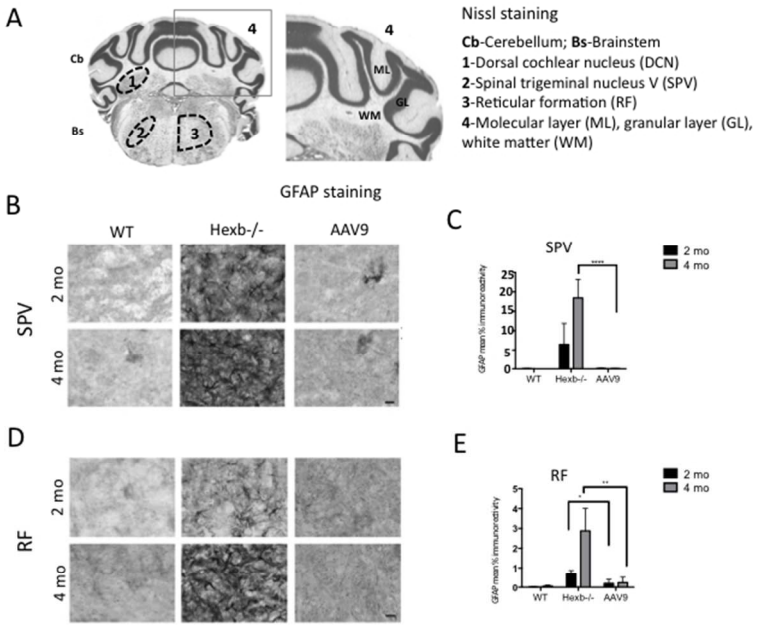

Figure 6

264x352mm (72 x 72 DPI)

Figure 7

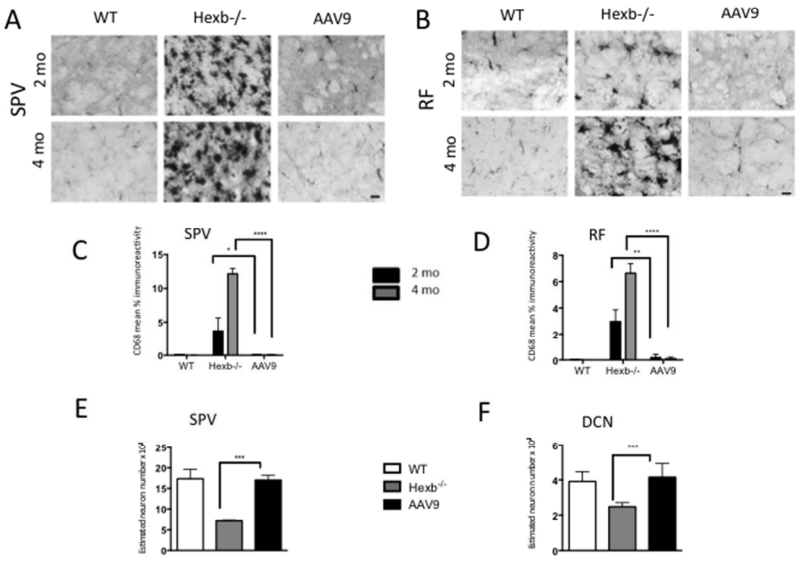

Figure 7

264x352mm (72 x 72 DPI)

Figure 8

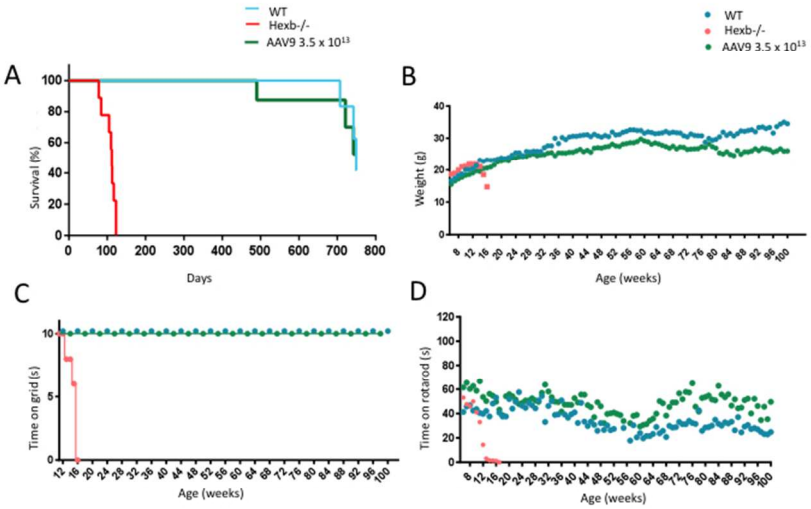

Figure 8

264x352mm (72 x 72 DPI)

Figure S1

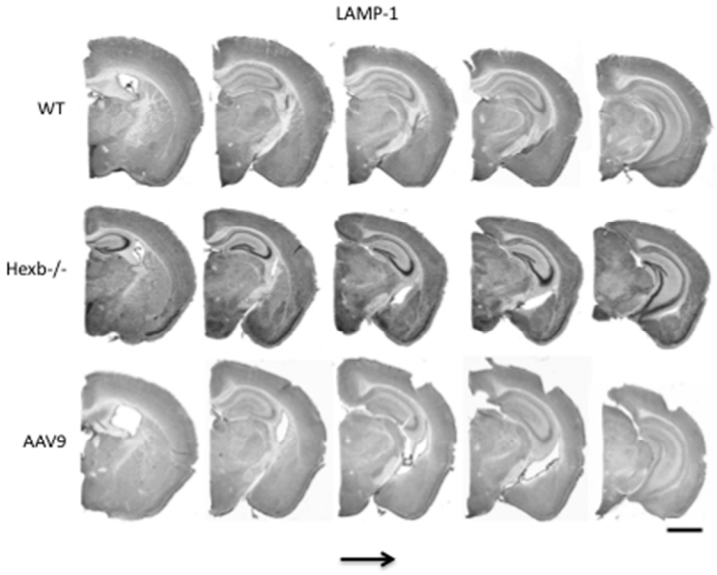

Figure S1

190x254mm (72 x 72 DPI)

Figure S2

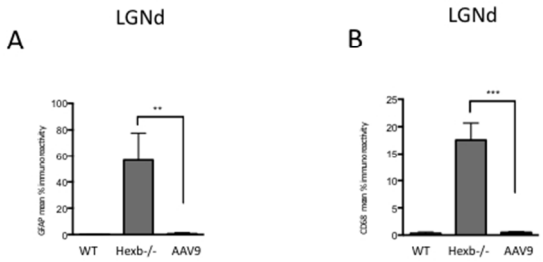

Supplementary figure 2

264x352mm (72 x 72 DPI)

Figure S3

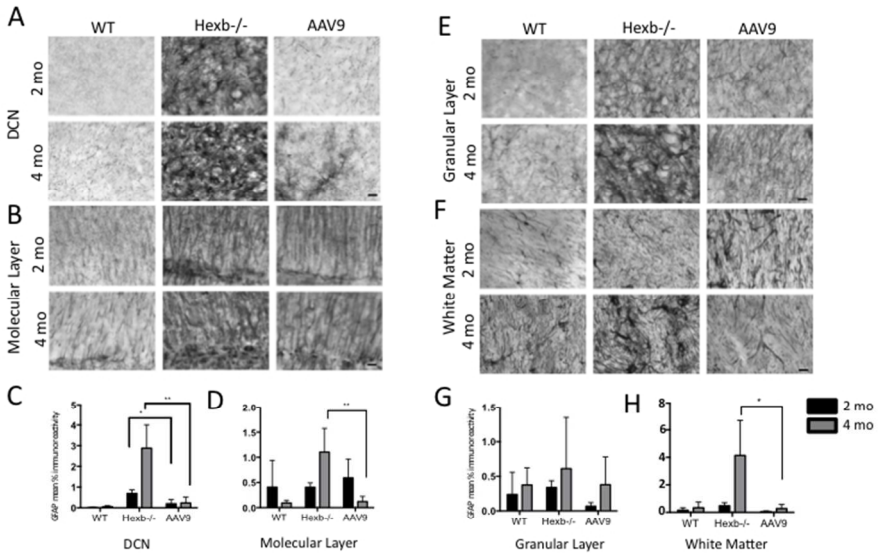

Supplementary figure 3

264x352mm (72 x 72 DPI)

Figure S4

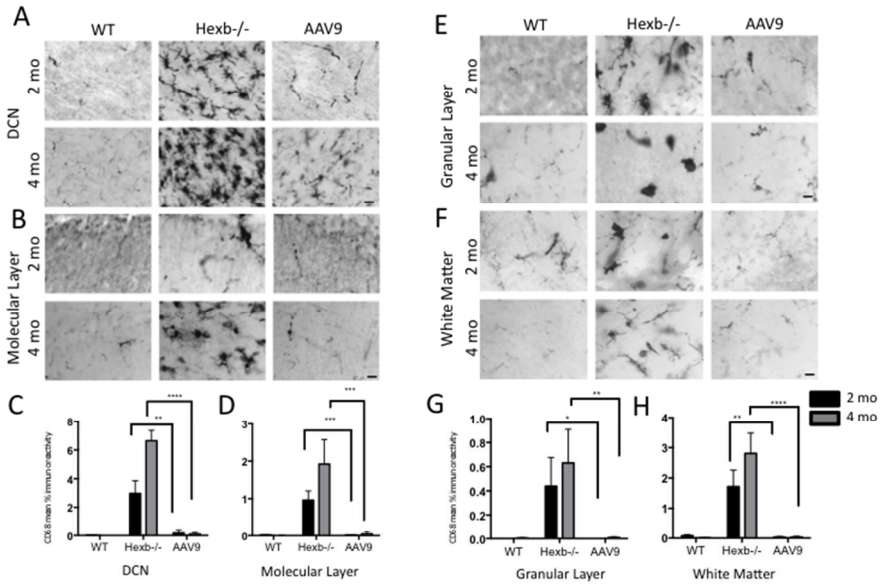

Supplementary figure 4

264x352mm (72 x 72 DPI)

Figure S5

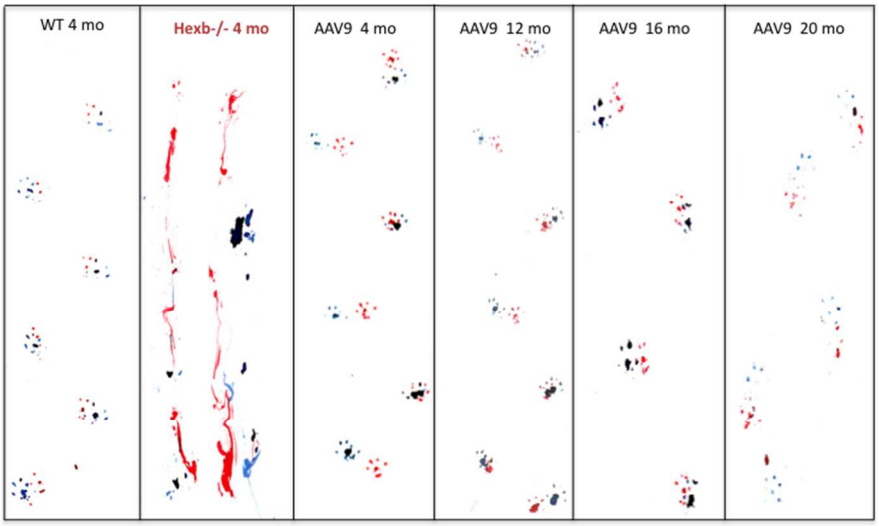

Supplementary figure 5

264x352mm (72 x 72 DPI)

Figure S6

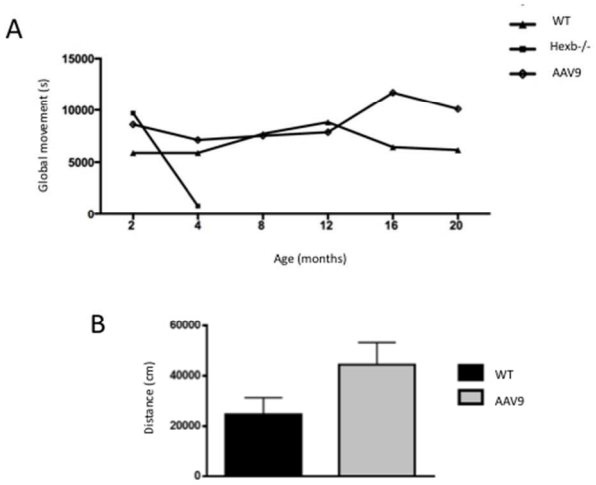

Supplementary figure 6

264x352mm (72 x 72 DPI)